GEOPHYSICS, VOL. 87, NO. 1 (JANUARY-FEBRUARY 2022); P. JM15–JM27, 11 FIGS., 1 TABLE.
10.1190/GEO2021-0307.1

Estimating the parameters of simple models from two-component on-time airborne electromagnetic data

Thomas Bagley[1] and Richard S. Smith[1]

ABSTRACT

The horizontal and vertical components of an on-time electromagnetic (EM) response can be used to estimate the parameters of simple models such as thin sheets, half-spaces, thin sheets over a lower half-space, and a two-layer model. The formulas used in these methods are valid in areas where the on-time response is essentially proportional to the conductivity or conductance, the so-called "resistive limit." The half-space and thin sheet over lower half-space models can be combined to give an estimate of the conductivity for a lower half-space below a thick sheet that might be reasonable for the entire survey area. With this estimation, an equation solver can be used to estimate the thickness and conductivity of the overlying thick sheet over the whole survey area. This latter approach seemed most appropriate for the Russell South area in the Athabasca Basin, Canada, where GEOTEM data have been collected. The output of the algorithm was generally stable. Although it did not always reliably reproduce the overburden thicknesses as measured in a set of reference drillholes, it did give an estimate that was reasonable in the relatively conductive areas.

INTRODUCTION

Active-source electromagnetic (EM) prospecting systems use a primary current flowing in a transmitter so as to excite the ground with a corresponding primary field (Grant and West, 1965). When this primary field varies as a function of time, secondary fields are induced in conductive bodies below the ground. This induced secondary field varies between two limits determined by the value of the dimensionless induction number $\omega\mu\sigma dl$, where ω is the angular frequency, μ is the permeability, σ is the conductivity, and d and l are the critical dimensions of the model and/or EM system depending on the model. For example, for the z-component response of the thin-sheet model, these critical dimensions are the thickness of the sheet and the sum of the transmitter and receiver heights, respectively (see equation 12 below). When the induction number is high, this is the inductive limit and secondary currents and fields are entirely in phase with the primary field. When the induction number is low, the secondary field is at the resistive limit, which is also called the low-induction-number regime in the near-surface geophysical community. At the resistive limit, the secondary response is proportional to the time derivative of the primary field, which is entirely out of phase or quadrature phase. These resistive-limit secondary fields do not interact with each other at the resistive limit, a fact first noted by Wait (1982), which is also demonstrated below. In between these two limits, there is an interaction between secondary currents, so the decay of a current will induce other secondary currents in conductive bodies. This results in a mixture of in-phase and quadrature phase fields in frequency-domain systems or in time-domain systems, gives a response that decays during the off time.

Traditional time-domain airborne EM (AEM) survey interpretation methods use only the off-time responses, which are measurements of the secondary field as it decays after the transmitter has been turned off. When there is an off-time decay, Grant and West (1965) show that the response of a thin conductive layer depends on the product of the conductivity-thickness (σt), so that the off-time response of a conductive overburden 30 m thick with conductivity of 1 S/m could not be easily distinguished from an overburden 15 m thick with conductivity of 2 S/m. A unique solution for the thickness or layer conductivity is not possible in this scenario using the off-time method. In this paper, we use resistive-limit methods that, in theory, might be able to resolve the thickness and conductivity of a layer. The resistive-limit approximation can be very useful in areas with overburden conductances up to 20 S or in areas where the conductivity of a half-space is up to 0.02 S/m because the resistive limit is proportional to the conductance or conductivity in a

Manuscript received by the Editor 11 May 2021; revised manuscript received 8 August 2021; published ahead of production 4 October 2021; published online 12 November 2021.
[1]Laurentian University, Harquail School of Earth Sciences, Sudbury, Ontario P3E 2C6, Canada. E-mail: bagleyt0@gmail.com; rssmith@laurentian.ca (corresponding author).

DOI:10.1190/geo2021-0307.1

linear fashion up to these values (Smith et al., 2005). Hence, these resistive-limit methods can be used in quite-conductive terrain, even when there is an off-time response. In parts of the Athabasca Basin, there is only an extremely weak off-time GEOTEM response at the earliest delay times, so on-time resistive-limit methods are the only realistic option.

On-time GEOTEM measurements have the primary or in-phase response removed and so are effectively time-domain quadrature measurements (Smith, 2001) and in resistive areas these can be well above noise levels (Annan et al., 1996; Smith, 2001). The resistive-limit measurements can also be estimated from frequency-domain systems by interpreting the quadrature response at low frequencies.

There are different formulas for deriving the physical properties of simple models of the earth from the resistive-limit responses. Annan et al. (1996) derive formula for estimating the conductivity of a half-space from the horizontal-component response. Their formulas converted a single component to get an estimate of a single parameter, the conductivity. If a vertical component is also measured, then these two measurements could be used to derive two independent estimates, but these might not be consistent. In this contribution, we consider an EM system that measures two or three components, as depicted in Figure 1, and we derive formulas for the half-space and the thin-sheet models, but for the horizontal (ρ) and vertical (z) component resistive-limit responses. If the ρ- and z-components are used to estimate the conductance of a thin sheet, and the two estimates happen to agree, then the responses are consistent with a thin-sheet model. Similarly, if both components happen to give a consistent estimate for the half-space conductivity, then a half-space model might be appropriate. Using the two components, it is sometimes possible to find a combination of the depth below the surface and the conductance (or conductivity) that gives the same estimate for both components. However, if this depth is less than the altimeter, then the assumed model is inappropriate because the model is above the ground surface.

If neither of the thin-sheet or half-space models are appropriate, then other models should be used. Hence, in this paper, we have also derived formulas for a thin sheet above a lower half-space and for a two-layer model (a thick sheet above a lower half-space). In this paper, we use the term *lower* half-space to describe a layer below a thin-sheet or thick-sheet overburden that extends to infinite depth, whereas henceforth we will use the term *simple* half-space to signify a model that has no overlying overburden.

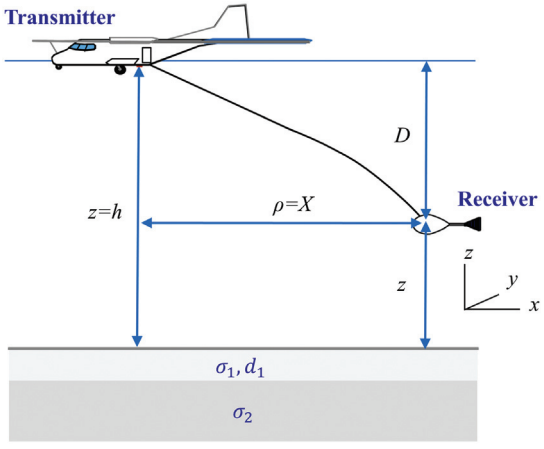

Figure 1. The EM system geometry over the two-layer model. The transmitter is mounted on an aircraft a vertical distance h above the ground surface, and the receiver is a distance D below and a radial distance X behind the transmitter. The receiver measures the response in three-component directions: one vertical z and two horizontal x and y. If the receiver flies straight and level behind the transmitter, then the horizontal component x is parallel to the radial component ρ.

If the depth below the surface of the thin sheet that lies above a lower half-space is assumed, then the ρ- and z-components can be used to estimate the conductance of the thin sheet and the conductivity of the lower half-space. If the estimated values are positive, then a thin sheet would be an appropriate model; if not, then we can use our thick-sheet model, but we must assume the depth to the top of the thick sheet and either assume that the lower half-space is highly resistive or estimate its conductivity using a procedure that we outline below.

In many cases, the earth can be approximated by a thin or thick layer over a lower half-space and an estimate of the appropriate model parameters is often desirable. In this contribution, we derive a formula that uses the x- and z-component data to estimate these parameters. However, these two measured components cannot be used to estimate more than two parameters, so some estimate or assumption must be made where there are more than two parameters characterizing the model. The most appropriate model to use will depend on the specific area where the data are collected. As an example, we tested the thick-sheet model on field data collected in the Athabasca Basin of Saskatchewan using the GEOTEM system. This area is challenging because the overburden and lower half-space are resistive, so the data are relatively noisy and there is no off-time response in much of the survey area. In this field example, we are investigating whether two-component (2C) on-time measurements can be used to estimate the thickness of the overburden. Knowing the thickness of the overburden can be important in the exploration process because it can be used to decide where to explore, the best location for siting drillholes, and in the Athabasca Basin it is considered important for correcting gravity data for variations in the depth of the overburden-bedrock surface (Braine and Macnae, 1999).

THEORY

The 2C thin-sheet and half-space derivations presented in this section follow the one-component derivation of Annan et al. (1996). The AEM system comprises a transmitter (T_x) positioned at an altitude $(z = h)$, above the ground. The transmitter is assumed to be a z-axis dipole, and the EM receiver (R_x) is composed of at least two dipolar induction coils, one oriented horizontally and the other vertically, so parallel to the ρ- and z-axes, respectively. The receiver coils are positioned a radial distance $(\rho = X)$ behind the aircraft and distance D vertically below the aircraft $(z = h - D)$. This system geometry is shown in Figure 1.

The primary field of the transmitter and the secondary field can be expressed in terms of a magnetic Hertz potential Π. For the case of the vertical-axis transmitter dipole, the Hertz potential has only a vertical component. The total Hertz potential is the sum of the primary and secondary:

$$\Pi = \Pi_p + \Pi_s, \tag{1}$$

where the primary field potential is the field of a unit dipole

DOI:10.1190/geo2021-0307.1

$$\Pi_p = \frac{1}{4\pi r} s(t) \tag{2}$$

and the secondary field potential is (Ward, 1967; Wait, 1982)

$$\Pi_s = \frac{1}{2\pi}\int_{-\infty}^{\infty} S(\omega) e^{i\omega t}\left[\int_0^{\infty} \frac{1}{4\pi} R(\lambda) e^{-\lambda(z+h)} J_0(\lambda\rho)\mathrm{d}\lambda\right]\mathrm{d}\omega. \tag{3}$$

The symbols for the above equations are provided in Table 1.

The radial H_ρ and vertical H_z components of the magnetic field are expressed as

$$H_\rho = \frac{\partial^2 \Pi}{\partial\rho\partial z}, \tag{4}$$

$$H_z = \frac{\partial^2 \Pi}{\partial z^2}. \tag{5}$$

Hence, the radial and vertical primary fields at the receiver are

$$H_\rho^P(t) = \frac{-3\rho(z-h)}{4\pi(\rho^2+(z-h)^2)^{5/2}} s(t) \tag{6}$$

and

$$H_z^P(t) = \frac{2(z-h)^2-\rho^2}{4\pi(\rho^2+(z-h)^2)^{5/2}} s(t). \tag{7}$$

RESISTIVE-LIMIT ANALYTICAL SOLUTIONS

In the resistive limit, the frequency or conductivity is sufficiently low that the eddy-current self interaction is negligible. Formally, this is written mathematically as $|\gamma_i/\lambda^2| \ll 1$ (Annan et al., 1996).

The conductive sheet model

If the conductivity of the second layer is zero and the thickness d_1 of the top layer is vanishingly small (while the conductivity-thickness product is finite) then (Wait, 1982)

$$\begin{aligned} \gamma_2 &= \lambda \\ \psi_1 &= \lambda - i\omega\mu\sigma_1 d_1. \end{aligned} \tag{8}$$

Therefore, the reflection coefficient simplifies to

$$R(\lambda) = \frac{i\omega\mu\sigma_1 d_1}{2\lambda}. \tag{9}$$

Taking the derivative with respect to z of the secondary Hertz potential, then the term in square brackets on the right side of equation 3 can be integrated using the Lipschitz-related integrals (Wait, 1982) to give the frequency-domain expression

$$\frac{\partial \Pi_S}{\partial z} = \frac{-i\omega\mu\sigma_1 d_1}{8\pi\sqrt{\rho^2+(z+h)^2}} S(\omega). \tag{10}$$

From equations 4, 5, and 10, we can write the secondary fields as

$$H_\rho^S = \frac{i\omega\mu\sigma_1 d_1 \rho}{8\pi[\rho^2+(z+h)^2]^{3/2}} S(\omega) \tag{11}$$

and

$$H_z^S = \frac{i\omega\mu\sigma_1 d_1 (z+h)}{8\pi[\rho^2+(z+h)^2]^{3/2}} S(\omega). \tag{12}$$

In both cases, the secondary field is purely imaginary, so it is by definition the quadrature phase. It also exhibits a linear increase with frequency, characteristic of the resistive limit. Multiplying by $i\omega$ is the equivalent of taking a time derivative in the time domain, so transforming these expressions to the time domain, we get

$$H_\rho^s(t) = \frac{\mu\sigma_1 d_1}{8\pi}\left[\frac{\rho}{(\rho^2+(z+h)^2)^{3/2}}\right]\frac{\mathrm{d}s(t)}{\mathrm{d}t}, \tag{13}$$

$$H_\rho^s(t) = \frac{\mu\sigma_1 d_1}{8\pi}\left[\frac{(z+h)}{(\rho^2+(z+h)^2)^{3/2}}\right]\frac{\mathrm{d}s(t)}{\mathrm{d}t}. \tag{14}$$

This result shows that at the resistive limit, there is no off-time response, as $\mathrm{d}s(t)/\mathrm{d}t = 0$ in the off time. Most importantly for

Table 1. Table of symbols.

$\gamma_n = (\lambda^2 - k_n^2)^{1/2}$	Vertical wavenumber in the nth layer
λ	Horizontal wavenumber
μ	Constant magnetic permeability
ρ	Radial coordinate
σ_n	Electrical conductivity of the nth layer, apparent conductivity derived from the nth component
ω	Angular frequency
d_n	Thickness of the nth layer
D	Vertical offset of receiver from transmitter
h	Vertical offset of transmitter from the top of the first layer
i	$\sqrt{-1}$
$k_n^2 = (i\omega\mu\sigma_n)$	Propagation constant in the nth layer
$r = (\rho^2 + (z-h)^2)^{1/2}$	Distance between the transmitter and receiver
$R(\lambda) = \frac{\lambda-\psi_1}{\lambda+\psi_1}$	Transverse-electric (TE) reflection coefficient
$s(t)$	Transmitter dipole moment waveform (Am^2)
$S(\omega)$	Transmitter dipole moment spectrum
$\psi_1 = \gamma_1 \frac{\gamma_2+\gamma_1\tanh(\gamma_1 d_1)}{\gamma_1+\gamma_2\tanh(\gamma_1 d_1)}$	Recursion formula for ψ_1 in the top layer
X	Radial offset of the receiver from the transmitter
z	Vertical coordinate above first layer

our methods, close to the resistive limit, the on-time response is proportional to the conductivity-thickness product $\sigma_1 d_1$ and this is also the case even when there is a moderate off-time response.

For a system that uses induction coil sensors, the measured voltage is proportional to the time rate of change of the magnetic flux $V = -\partial\phi/\partial t$, where the flux $\phi = AB$ and B is the magnitude of the magnetic flux density cutting the coil and A is the area of the receiver coil. As $\mathbf{B} = \mu\mathbf{H}$, then the voltage measured in the coil is

$$V_i^j = \sigma_1 d_1 G_i^{\mathrm{TS}}(z,\rho,h)\frac{d^2 s(t)}{dt^2}, \tag{15}$$

where the subscript i denotes the appropriate component and the relevant formula for the G_i^{TS} is

$$G_\rho^{\mathrm{TS}}(z,\rho,h) = \frac{\mu^2 A}{8\pi}\left[\frac{\rho}{(\rho^2+(z+h)^2)^{3/2}}\right], \tag{16}$$

$$G_z^{\mathrm{TS}}(z,\rho,h) = \frac{\mu^2 A}{8\pi}\left[\frac{(z+h)}{(\rho^2+(z+h)^2)^{3/2}}\right], \tag{17}$$

and for the airborne systems $\rho = X$ and $z = h - D$.

Because the GEOTEM and MEGATEM waveforms can be represented by a half-sine pulse of the dipole moment, which starts at $t = 0$ and ends at $t = P$, such that

$$s(t) = S_0 \sin\left(\frac{\pi t}{P}\right) \tag{18}$$

during the pulse and $s(t) = 0$ elsewhere. The maximum dipole moment is in the middle of the pulse at $t = P/2$ and has a magnitude of S_0 and units of Am^2. Differentiating this once, we get

$$\frac{ds(t)}{dt} = S_0\frac{\pi}{P}\cos\left(\frac{\pi t}{P}\right)[u(t) - u(t-P)], \tag{19}$$

where $u(t)$ is the unit step-on function (unity for positive arguments), here being used to ensure that the derivative of the dipole moment waveform is nonzero (on) between $t = 0$ and $t = P$ and off otherwise. Differentiating this again, we get

$$\frac{d^2 s(t)}{dt^2} = S_0\left[\frac{\pi}{P}\cos\left(\frac{\pi t}{P}\right)[\delta(t) - \delta(t-P)] - \left(\frac{\pi}{P}\right)^2 \sin\left(\frac{\pi t}{P}\right)[u(t) - u(t-P)]\right], \tag{20}$$

where $\delta(t)$ is the Dirac delta function. From this we can see that the earth response in the resistive limit is a large spike at the transmitter switch on at $t = 0$ and another at the transmitter switch off at $t = P$ and a half-sine function between these two pulses (Annan et al., 1996). Consequently, the initial on-time measurement window 1 used with the GEOTEM and MEGATEM was placed at the start of the waveform centered on $t = t_1$. Integrating expression 20 over a narrow window of aperture ε, centered at time $t = t_1$ yields the required observed on-time signal,

$$O_i = \frac{1}{\varepsilon}\int_{t_1-\varepsilon/2}^{t_1+\varepsilon/2} V_i(t)dt, \tag{21}$$

$$= \frac{\sigma_1 d_1 \pi G_i^{\mathrm{TS}} S_0}{\varepsilon P}. \tag{22}$$

The resulting expression can be rearranged to yield an expression for the conductance of the thin sheet

$$\sigma_1 d_1 = \frac{\varepsilon P O_i}{\pi G_i^{\mathrm{TS}} S_0}. \tag{23}$$

To ensure that the resultant expression has the units of siemens, the ε and P must be in s, O_i in volts, G_i^{TS} in $\mathrm{kg^2 s^{-4} A^{-4} m^2}$, and S_0 in Am^2. The GEOTEM and MEGATEM voltage responses are often reported in $\mathrm{pV/m}^2$, which is the voltage already divided by the area of the receiver coil, making this effectively a receiver coil with a unit area. Hence, A in expressions 16 or 17 should be set to $1\mathrm{m}^2$ and the voltage in $\mathrm{pV/m}^2$ should be converted to $\mathrm{V/m}^2$.

Because the geologic setting will seldom truly be a thin sheet, the name "on-time apparent conductance" is used. The thin sheet will not always lie at the surface or be above a highly resistive lower half-space, so the estimate of the conductance $S_\rho = \sigma_1 d_1$ from the ρ-component and the conductance $S_z = \sigma_1 d_1$ from the z-component will in these cases not be equal. If we assume that the lower half-space has a zero conductivity, then we can set $S_\rho = S_z$ and solve for a new value for

$$h = \frac{1}{2}\left(D + X\frac{O_z}{O_\rho}\right), \tag{24}$$

the altitude of the transmitter above the thin sheet. Substituting back into equation 23 using either the ρ- or z-component should give the same value of conductance from both components. The altitude given in equation 24 should be greater than or equal to the altimeter reading because the thin sheet should be below the terrain. If it is not, or the conductance is negative, then the amplitude of the z- and ρ-component responses is not consistent with the thin-sheet model and another model might be more appropriate.

Half-space model

If the model is a half-space, then

$$\begin{aligned} d_1 &= 0, \\ \psi_1 &= \gamma_1. \end{aligned} \tag{25}$$

At the resistive limit, the reflection coefficient becomes

$$R(\lambda) \approx \frac{i\omega\mu\sigma_2}{4\lambda^2}, \tag{26}$$

which again allows the field expressions to be integrated analytically. The Hankel transform integral for the resistive limit is well discussed by Wait (1982), and in the specific case of a half-space, it yields the following expression for the H_ρ and H_z secondary responses:

$$H_\rho^S(\omega) = \frac{i\omega\mu\sigma_2}{16\pi\rho}\left[1 - \frac{z+h}{(\rho^2+(z+h)^2)^{1/2}}\right]S(\omega), \quad (27)$$

$$H_z^S(\omega) = \frac{i\omega\mu\sigma_2}{16\pi}\left[\frac{1}{(\rho^2+(z+h)^2)^{1/2}}\right]S(\omega), \quad (28)$$

which become on transformation to the time domain

$$H_\rho^S(t) = \frac{\mu\sigma_2}{16\pi\rho}\left[1 - \frac{z+h}{(\rho^2+(z+h)^2)^{1/2}}\right]\frac{\mathrm{d}s(t)}{\mathrm{d}t}, \quad (29)$$

$$H_z^S(t) = \frac{\mu\sigma_2}{16\pi}\left[\frac{1}{(\rho^2+(z+h)^2)^{1/2}}\right]\frac{\mathrm{d}s(t)}{\mathrm{d}t}. \quad (30)$$

Note once again that the response is proportional to the half-space conductivity.

Proceeding similarly to the conductive sheet model, we can write

$$\sigma_2 = \frac{\varepsilon PO_i}{\pi G_i^H S_0}, \quad (31)$$

where

$$G_\rho^H(z,\rho,h) = \frac{\mu^2 A}{16\pi\rho}\left[1 - \frac{z+h}{(\rho^2+(z+h)^2)^{1/2}}\right], \quad (32)$$

$$G_z^H(z,\rho,h) = \frac{\mu^2 A}{16\pi}\left[\frac{1}{(\rho^2+(z+h)^2)^{1/2}}\right], \quad (33)$$

and for the airborne systems $\rho = X$ and $z = h - D$.

Once again, the ρ- and z-components can be used to give the half-space apparent conductivity. However, there is no guarantee that the values obtained will be the same. It is possible to show that the ρ- and z-components will give a consistent value if

$$h = \frac{1}{2}\left[D - \frac{X}{2\alpha}(\alpha^2 - 1)\right], \quad (34)$$

where

$$\alpha = \frac{O_\rho}{O_z}. \quad (35)$$

If the conductivity for this height is negative or the height less than the altimeter reading, then the half-space model might not be appropriate.

Thin sheet overlying a lower half-space model

If the model is comprised of a thin conductive sheet at the surface overlying a conductive lower half-space, then at the resistive limit

$$\psi_1 = \sqrt{\lambda^2 - i\omega\mu\sigma_2} - i\omega\mu\sigma_1 d_1 \quad (36)$$

and

$$R(\lambda) = \frac{i\omega\mu\sigma_2}{4\lambda^2} + \frac{i\omega\mu\sigma_1 d_1}{2\lambda}. \quad (37)$$

By inspection, the reflection coefficient is the sum of the thin-sheet and half-space reflection coefficients, so the measured response can be written as

$$\frac{\varepsilon PO_\rho}{\pi S_0} = \sigma_1 d_1 G_\rho^{\mathrm{TS}} + \sigma_2 G_\rho^H, \quad \frac{\varepsilon PO_z}{\pi S_0} = \sigma_1 d_1 G_z^{\mathrm{TS}} + \sigma_2 G_z^H, \quad (38)$$

where the superscripts TS and H denote the geometry factors for the thin-sheet and half-space in equations 16 and 17 and equations 32 and 33, respectively. This is a linear system of equations, the solution to which is

$$\begin{pmatrix}\sigma_1 d_1\\ \sigma_2\end{pmatrix} = \frac{1}{G_\rho^{\mathrm{TS}} G_z^H - G_z^{\mathrm{TS}} G_\rho^H}\begin{pmatrix} G_z^H & -G_\rho^H \\ -G_z^{\mathrm{TS}} & G_\rho^{\mathrm{TS}}\end{pmatrix}\begin{pmatrix}\frac{\varepsilon O_\rho P}{\pi S_0}\\ \frac{\varepsilon O_z P}{\pi S_0}\end{pmatrix}. \quad (39)$$

Valid solutions to this inversion will have the conductance and the conductivity as positive. Note that we are assuming that the geometry factors are known, so we must specify the depth h to the thin sheet and lower half-space.

Contribution of material from different depths

A half-space sensitivity analysis is performed for the purposes of determining the contribution of the material at each depth to the response and hence the apparent conductivity. This will be used below for deriving formulas for a thick sheet.

If the substitution

$$\psi_1 = \frac{1}{Q} \quad (40)$$

is made, then the reflection coefficient in Table 1 becomes

$$R(\lambda) = \frac{\lambda Q - 1}{\lambda Q + 1} \quad (41)$$

and

$$\frac{\partial R(\lambda)}{\partial Q} = \frac{2\lambda}{(\lambda Q + 1)^2}. \quad (42)$$

In the resistive limit, $\psi_1 \approx \lambda$, so

$$\frac{\partial R(\lambda)}{\partial Q} = \frac{\lambda}{2}. \quad (43)$$

The change in Q resulting from integrating small changes in the conductivity at a depth z' is (Parker, 1977; Edwards and Cheesman, 1987; Smith et al., 1994)

$$\delta Q = \int_0^\infty i\omega\mu \frac{e^{-2\psi_1 z'}}{\psi_1^2}\delta\sigma(z')\mathrm{d}z', \tag{44}$$

where in this section the conductivity of the half-space is denoted as σ. If the resistive-limit approximation is made and fractional changes in the conductivity are considered, then

$$\delta Q = \int_0^\infty i\omega\mu\sigma \frac{e^{-2\lambda z'}}{\lambda^2}\delta \ln \sigma(z')\mathrm{d}z'. \tag{45}$$

The fractional change in $\partial\Pi/\partial z$ is then

$$\begin{aligned}\delta(\partial\Pi/\partial z) &= \frac{\partial(\partial\Pi/\partial z)}{\partial Q}\delta Q \\ &= \frac{-i\omega\mu\sigma}{8\pi}\int_0^\infty e^{-\lambda(z+h)}J_0(\lambda\rho)\mathrm{d}\lambda \int_0^\infty e^{-2\lambda z'}\delta \ln \sigma(z')\mathrm{d}z'.\end{aligned} \tag{46}$$

As the only perturbation of interest is a unit fractional change in the conductivity at depth z', then $\delta \ln \sigma = \delta(z')$, where $\delta(z')$ is the Dirac delta function. Thus, equation 46 becomes

$$\delta(\partial\Pi/\partial z) = \frac{-i\omega\mu\sigma}{8\pi}\left[\frac{1}{\sqrt{\rho^2+(z+h+2z')^2}}\right], \tag{47}$$

which can be used to give the sensitivities for the ρ- and z-components using equations 4 and 5

$$\delta H_\rho = \frac{i\omega\mu\sigma}{8\pi}\left[\frac{\rho}{[\rho^2+(z+h+2z')^2]^{3/2}}\right], \tag{48}$$

$$\delta H_z = \frac{i\omega\mu\sigma}{8\pi}\left[\frac{z+h+2z'}{[\rho^2+(z+h+2z')^2]^{3/2}}\right]. \tag{49}$$

Note that these are the formulas for the magnetic field of a thin sheet when z and h have been replaced by $z+z'$ and $h+z'$, respectively.

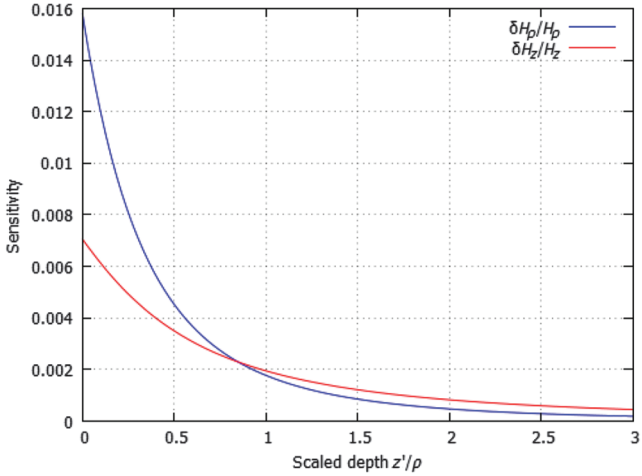

Figure 2. Sensitivity of the ρ- (blue) and z-components (red) to changes in the conductivity of a half-space at a specific scaled depth $z_a = z'/\rho$.

This shows that, in the resistive limit, a unit fractional change in the conductivity at depth z' is the same as the resistive-limit response of a thin sheet at the same depth. Because the thin sheet is by definition surrounded by nonconducting material that it does not interact with, this shows that the perturbation is not interacting with the other material in the half-space. This demonstrates that in the resistive limit, there is no interaction between the conductive material. The normalized sensitivities are

$$\frac{\delta H_\rho}{H_\rho} = \frac{2\rho^2}{[\rho^2+(z+h+2z')^2]^{3/2}\left[1-\frac{(z+h)}{(\rho^2+(z+h)^2)^{1/2}}\right]} \tag{50}$$

and

$$\frac{\delta H_z}{H_z} = \frac{2(z+h+2z')\sqrt{\rho^2+(z+h)^2}}{[\rho^2+(z+h+2z')^2]^{3/2}}. \tag{51}$$

To simplify these equations and make them less dependent on specific length parameters, we apply scaling similar to that used by McNeill (1980, Geonics Ltd. Tech., note TN-6) and define scaled variables $z_s = (z+h)/\rho$ and $z_a = z'/\rho$, so that equations 50 and 51 become

$$\frac{\delta H_\rho}{H_\rho} = \frac{2}{\rho[1+(z_s+2z_a)^2]^{3/2}\left[1-\frac{z_s}{(1+z_s^2)^{1/2}}\right]} \tag{52}$$

and

$$\frac{\delta H_z}{H_z} = \frac{2(z_s+2z_a)\sqrt{1+z_s^2}}{\rho[1+(z_s+2z_a)^2]^{3/2}}. \tag{53}$$

For the case in which $z = h = 0$, the latter of the two equations reduces to that stated by McNeill (1980, Geonics Ltd. Tech., note TN-6), but it is actually not derived. These functions are plotted in Figure 2 for the case in which $X = 135$ m and $2h - D = 185$ m, hereafter called the *nominal geometry*.

The depth at which the z- and ρ-components have equal sensitivities can be obtained by equating equations 52 and 53. This gives

$$z' = \rho z_a = \frac{\rho}{2}\sqrt{1+z_s^2}, \tag{54}$$

which is approximately 115 m for the standard configuration. The conductivity more strongly influences the ρ-component at depths shallower than 115 m; the z-component has greater influence at depths greater than 115 m.

Model with two layers

An important function for interpreting the effect of subsurface conductivity is the cumulative response defined by McNeill (1980, Geonics Ltd. Tech., note TN-6):

$$R_i(z') = \int_{z'}^\infty \frac{\delta H_i}{H_i}\mathrm{d}z, \tag{55}$$

where $i = \rho$ or z. Integrated analytically, this gives

$$R_p(z_a) = \frac{\left[1 - \frac{z_s+2z_a}{\sqrt{1+(z_s+2z_a)^2}}\right]}{\left[1 - \frac{z_s}{\sqrt{1+z_s^2}}\right]}, \tag{56}$$

$$R_z(z_a) = \frac{\sqrt{1+z_s^2}}{\sqrt{1+(z_s+2z_a)^2}}, \tag{57}$$

where z_s and z_a are defined before equation 52.

These functions have been plotted in Figure 3. McNeill (1980, Geonics Ltd. Tech., note TN-6) somewhat arbitrarily defines the depth of exploration as the depth at which the cumulative response is equal to 0.3. From Figure 3, this gives scaled depths of 0.75 and 2.1 for the radial and vertical components, respectively. For the nominal geometry, this corresponds to depths of 100 and 284 m.

The power of the cumulative response function is that it can be used to relate the actual conductivity as a function of depth to the apparent conductivity (McNeill, 1980, Geonics Ltd. Tech., note TN-6). The relationship exists because there is no mutual interaction between material at different depths.

For a two-layer earth, the ρ- and z-component apparent conductivity can be written as

$$\begin{aligned}\sigma_\rho^a &= \sigma_1(1 - R_\rho(d_1)) + \sigma_2 R_\rho(d_1),\\ \sigma_z^a &= \sigma_1(1 - R_z(d_1)) + \sigma_2 R_z(d_1),\end{aligned} \tag{58}$$

where σ_1 and d_1 are the conductivity and thickness of the top layer, respectively, and σ_2 is the conductivity of the lower half-space. This is a set of two nonlinear equations in three unknowns. These equations can be solved in a least-squares sense using nonlinear solvers, but they can also be solved more elegantly for several specific models, as will be illustrated below.

Thick-sheet model

If the conductivity of the lower half-space, σ_2, is assumed to be zero, then σ_1 can be eliminated from equation 58 to give

$$f(d_1) = \frac{1 - R_\rho(d_1)}{1 - R_z(d_1)} - \frac{\sigma_\rho^a}{\sigma_z^a} = 0. \tag{59}$$

The first term of $f(d_1)$ is monotonically decreasing, so this equation can be solved for d_1 with a simple root finder (e.g., Brent's method). However, a solution exists for a limit range of the ratio σ_ρ/σ_z. The first term goes to 1 as $d_1 \to \infty$; as $d_1 \to 0$ the limiting value can be found by using a Taylor series expansion:

$$\lim_{d_1\to 0}\frac{1 - R_\rho(d_1)}{1 - R_z(d_1)} = \frac{1 - (R_\rho(0) + d_1\frac{\mathrm{d}R_\rho}{\mathrm{d}d_1}|_{d_1=0})}{1 - (R_z(0) + d_1\frac{\mathrm{d}R_z}{\mathrm{d}d_1}|_{d_1=0})} = \frac{\frac{\mathrm{d}R_\rho}{\mathrm{d}d_1}|_{d_1=0}}{\frac{\mathrm{d}R_z}{\mathrm{d}d_1}|_{d_1=0}}. \tag{60}$$

From equations 56 and 57

$$\frac{\mathrm{d}R_\rho}{\mathrm{d}z_a} = \frac{-2}{\left(1 - \frac{z_s}{\sqrt{1+z_s^2}}\right)(1+(z_s+2z_a)^2)^{3/2}} \tag{61}$$

and

$$\frac{\mathrm{d}R_z}{\mathrm{d}z_a} = \frac{-2(z_s+2z_a)\sqrt{1+z_s^2}}{(1+(z_s+2z_a)^2)^{3/2}}, \tag{62}$$

which gives

$$\lim_{d_1\to 0}\frac{1 - R_\rho(d_1)}{1 - R_z(d_1)} = \frac{1}{z_s\sqrt{1+z_s^2} - z_s^2} \tag{63}$$

for the normal geometry, this limiting value is equal to 2.24. Thus, for a thick-sheet solution to exist, it is required that

$$1 \le \sigma_\rho/\sigma_z \le 2.24. \tag{64}$$

Once d_1 has been found by solving equation 59, σ_1 can be found by substituting into either of the equations in equation 58.

Known thickness

If the thickness is known, assumed, or selected from equation 54, then the equations in equation 58 reduce to a set of linear equations, the solution to which is

$$\begin{pmatrix}\sigma_1\\ \sigma_2\end{pmatrix} = \frac{1}{R_z - R_\rho}\begin{pmatrix}R_z & -R_\rho\\ -(1-R_z) & 1-R_\rho\end{pmatrix}\begin{pmatrix}\sigma_\rho\\ \sigma_z\end{pmatrix}. \tag{65}$$

This equation is nonsingular unless $R_z = R_\rho$. This only occurs when $R_z = R_\rho = 1$, in which case the ground is a half-space with $\sigma_z = \sigma_\rho$, and no inverse is required. The application of equation 65 does not ensure that the resulting conductivities σ_1 and σ_2 are positive. In the case of negative conductivities, the assumed model or thickness is not valid.

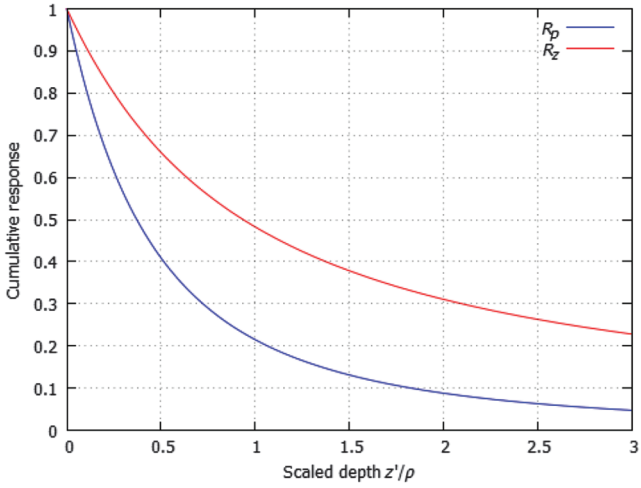

Figure 3. Cumulative response functions for the ρ- (blue) and the z-components (red).

Known top-layer conductivity

If σ_1 is assumed, then the unknowns are σ_2 and d_1. The term σ_2 can be eliminated from the equations in equation 58 to give

$$f(d_1) = \frac{R_\rho(d_1)}{R_z(d_1)} - \frac{\sigma_\rho - \sigma_1}{\sigma_z - \sigma_1} = 0, \tag{66}$$

which can be solved for d_1 using standard root-finding methods. The ratio R_ρ/R_z is a monotonically increasing function in the range $[0, 1]$. Hence, for there to be a solution, we require that

$$0 \le \frac{\sigma_\rho - \sigma_1}{\sigma_z - \sigma_1} \le 1. \tag{67}$$

The first (positive) inequality tells us that if $\sigma_z > \sigma_1$ then $\sigma_\rho > \sigma_1$, or if $\sigma_z < \sigma_1$ then $\sigma_\rho < \sigma_1$. From the second (less-than-unity) inequality, if the bottom line is positive, then $\sigma_z > \sigma_1$ and, hence, $\sigma_z > \sigma_\rho$. Similarly, if the bottom line is negative, then $\sigma_z < \sigma_1$ and, hence, $\sigma_z < \sigma_\rho$. If a root exists, σ_2 can be found by back substitution into one of the equations in equation 58. If there are high-quality early off-time data over the whole survey area, then these data could be used to estimate σ_1.

Known lower half-space conductivity

If σ_2 is assumed, then σ_1 and d_1 are unknown. Eliminating σ_1 from the equations in equation 58 gives

$$f(d_1) = \sigma_\rho - \sigma_z + R_z(d_1)(\sigma_2 - \sigma_\rho) + R_\rho(d_1)(\sigma_z - \sigma_2) = 0. \tag{68}$$

Again, this can be solved for d_1 using a standard root finder, and σ_1 can be found by back substitution. In the limit $d_1 \to 0$, $f(d_1) = 0$; however, this is not the required solution because this reduces to the half-space case. The function $f(d_1)$ is more complicated and requires more analysis to determine when there is a solution. Writing

$$f(d_1) = \sigma_\rho - \sigma_z + R_z(d_1)\alpha + R_\rho(d_1)\beta, \tag{69}$$

where $\alpha = \sigma_2 - \sigma_\rho$ and $\beta = \sigma_z - \sigma_2$. Turning points of $f(d_1)$ can be found by setting $\mathrm{d}f(d_1)/\mathrm{d}d_1 = 0$, which can be solved using equations 61 and 62 to give a single turning point

$$d_1 = -\left(z_s + \frac{\beta}{\alpha[z_s + \sqrt{1 + z_s^2}]}\right). \tag{70}$$

The only realistic turning points are for $d_1 > 0$, so

$$\frac{\beta}{\alpha} < -z_s\left(z_s + \sqrt{1 + z_s^2}\right). \tag{71}$$

The sign of $f(d_1)$ prior to the turning point can be ascertained by determining the slope of $f(d_1)$ at $d_1 = 0$. Specifically,

$$\frac{\mathrm{d}f(d_1)}{\mathrm{d}d_1}\Big|_{d_1=0} = \frac{-[\alpha z_2\sqrt{1 + z_s^2} + \alpha z_s^2 + \beta]}{(1 + z_s^2)^{3/2}(1 + z_s(1 + z_s^2)^{-1/2})}. \tag{72}$$

The slope is positive if the term in square brackets is negative, and the slope is negative if the term in square brackets is positive. If the term in square brackets is zero, the turning point is at $d_1 = 0$ and there are no other solutions. The value of the function $f(d_1)$ at $d_1 = \infty$ is $\sigma_\rho - \sigma_2$. Hence, there is a solution to equation 68 if

1) the slope of $f(d_1)$ is positive at $d_1 = 0$, there is a turning point $d_1 \epsilon (0, \infty]$, and $\sigma_\rho - \sigma_z$ is negative,
2) the slope of $f(d_1)$ is negative at $d_1 = 0$, there is a turning point $d_1 \epsilon (0, \infty]$, and $\sigma_\rho - \sigma_z$ is positive.

If there is no solution, then one of the other models is more appropriate.

Newtonian root finder for σ_2 known

In the following, rather than solve equation 68, we are going to use a Newtonian root finder to estimate the conductivity and thickness of a thick layer over a lower half-space for the case of known lower half-space conductivity. This involves using the familiar Newton-Raphson method for multiple variables

$$\begin{bmatrix} \frac{\partial O_\rho}{\partial \sigma_1} & \frac{\partial O_\rho}{\partial d_1} \\ \frac{\partial O_z}{\partial \sigma_1} & \frac{\partial O_z}{\partial d_1} \end{bmatrix} \begin{bmatrix} \Delta\sigma_1 \\ \Delta d_1 \end{bmatrix} = -\begin{bmatrix} O_\rho^n - O_\rho^m \\ O_z^n - O_z^m \end{bmatrix}, \tag{73}$$

where O_i^m is the measured response for the ith component, O_i^n is the calculated responses of an initial guess or previous iteration n, and $\Delta\sigma_1 = \sigma_1^n - \sigma_1^{n+1}$ and $\Delta d_1 = d_1^n - d_1^{n+1}$ are the differences between the previous or initial guesses and the next updates $(n + 1)$. These differences can be solved using the inverse of a two-by-two matrix and the update obtained, namely,

$$\begin{aligned} \Delta\sigma_1 &= \frac{1}{\mathcal{D}}\left[(O_\rho^n - O_\rho^m)\frac{\partial O_z}{\partial d_1} - (O_z^n - O_z^m)\frac{\partial O_\rho}{\partial d_1}\right], \\ \Delta d_1 &= \frac{1}{\mathcal{D}}\left[(O_z^n - O_z^m)\frac{\partial O_\rho}{\partial \sigma_1} - (O_\rho^n - O_\rho^m)\frac{\partial O_z}{\partial \sigma_1}\right], \end{aligned} \tag{74}$$

where

$$\mathcal{D} = \frac{\partial O_\rho}{\partial d_1}\frac{\partial O_z}{\partial \sigma_1} - \frac{\partial O_\rho}{\partial \sigma_1}\frac{\partial O_z}{\partial d_1} \tag{75}$$

is the determinant of the matrix. It is also possible to modify the partial derivatives to yield solutions for the cases in which σ_1, σ_2, and d_1 are known. In our field example, the root-finding algorithm was sensitive to measurement noise, but we found that this could be minimized by leveling the input data using the Geosoft Oasis Montaj microleveling procedures. This was done to remove strong features that ran along the lines and were clearly not geologic. We also found that stable results could be obtained by reducing the changes in the model parameters at each iteration by multiplying the changes suggested by the inversion algorithm by a number less than one. In our paper, we found that multiplication by 0.05 resulted in stable estimates.

FIELD EXAMPLE, RUSSELL SOUTH

Uranium exploration and geologic setting

The Russell South property is located in the southeastern Athabasca Basin, which is notably prospective for uranium. The

DOI:10.1190/geo2021-0307.1

basement below the Athabasca Basin is the Hearne craton, and above an unconformity lies the Proterozoic metasediments of the Athabasca Group. Uranium deposits exist in the Athabasca Basin in the presence of structural complexity, through which fluids were permeated and uranium was deposited at economic grades in the form of uraninite. It is close to the unconformity between the Hearne and the Proterozoic metasediments that the deposits are normally found, often near a graphitic seam that is present in the Hearne. In the deposit model, there also exists a halo of alteration where the gangue rock has reacted with the same fluids to form clay. The thickness of the Proterozoic metasediment package can be up to 2 km, meaning that some deep deposits probably lie undiscovered (Jefferson et al., 2007). At the Russell South property, the depth to the unconformity is approximately 100 m in the south to 250 m in the north (Robertshaw, 2006).

Quaternary sediments exist in the area and are likely to be the principal geologic control on the topography. These sediments, primarily a consequence of recent glaciation, comprise moraines, eskers, drumlins, and lake sediments. Quaternary sediments are henceforth referred to as overburden because they have had no influence upon the genesis of uranium, and their variable thickness can be a source of geologic noise for some exploration methods. In particular, changes in the thickness can have an impact on the gravity response that could obscure the gravity response of any identifying alteration that might be present (Darijani, 2019).

GEOTEM data set

GEOTEM AEM data were collected between 10 March 2005 and 16 March 2005 by Fugro Airborne Surveys on behalf of Roughrider Uranium Corporation using a modified Casa 212 aircraft. The data and the survey equipment specifications can be found in the report by Fugro (2005), both of which were filed for assessment with the Geological Survey of Saskatchewan (GSS) by Roughrider and are publicly available from the GSS website.

Figure 4 illustrates the high-altitude (primary) waveforms measured at the receiver for the x-, y-, and z-components. Window 1 is the on-time window with the steepest primary response and is hence the window that, once the derivative of the waveform is taken, provides the best approximation of a Dirac delta function (Smith, 2000). Hence, it was the window chosen for interpretation.

AEM has been used extensively in the Athabasca Basin to search for the graphite shear zones in the basement, and this was the purpose of the Russell South survey flown in 2005 with a line spacing of 300 m. Because the graphite shear zones are very conductive, they are easily distinguishable in the off-time measurement windows. Because the goal of the survey was to measure conductive features in the off-time, little emphasis appears to have been put upon the leveling and filtering of the on-time windows. A triangular filter with a width of 91 points was applied to remove bird-swing pendulum effects. A similar filter was applied to the same data set by Smith and Lee (2021), who also discuss the pendulum effects in more detail. If this noise is ignored, it upsets the stability of the Newton-Raphson root finder.

The Russell South area is highly resistive, with more than 50% of the area having no GEOTEM response above the noise levels in the off-time windows (Fugro, 2005; Smith and Lee, 2021). Because traditional 1D and 3D EM inversion methods use the off-time data, these methods cannot be used to estimate the overburden thickness and create a map of the thickness over the whole survey area. For this reason, we are only able to use the resistive-limit methods described in this paper to get estimates because we can use the on-time data, which are largely greater than the noise level.

Inversion to sheet thickness

The Newton-Raphson inversion procedure was applied to invert for sheet thickness and conductivity using the known lower half-space conductivity method. The lower half-space conductivity was first estimated by comparing the ρ- and z-component solutions for the half-space conductivity. When these two solutions agreed to within 1% of each other, the model is effectively a half-space with no conductive overburden, so these estimates were deemed to be valid estimates of the lower half-space conductivity. We found that the lower half-space conductivity determined in this way was generally approximately 0.0003 S/m or less, so we set the lower half-space conductivity everywhere to the average of all the values that agree to closer than 1%, which gives an average value of 0.00295 S/m.

The inversion code was written in C and first tested to be self-consistent against synthetic models (Bagley and Smith, 2018). Once deemed internally consistent, it was then applied to the Russell South data set and the output was imaged in Oasis Montaj. The processing and inversion steps are summarized by the flowchart presented in Figure 5.

The response in the z- and x-components is shown in Figures 6 and 7. These images were gridded using the minimum curvature method. Some residual leveling errors are still evident, running parallel to the flight lines at 120°–300°. The z- and x-components show similar shaped features, so the response is likely associated with large flat-lying features such as overburden. In the following, we have assumed that the x-component is the ρ-component, which is a good approximation in a layered environment. The altitude, measured with the GPS system, and the height above terrain, measured with the radar altimeter on the GEOTEM aircraft, have been used to estimate the digital terrain model (DTM), which is shown in

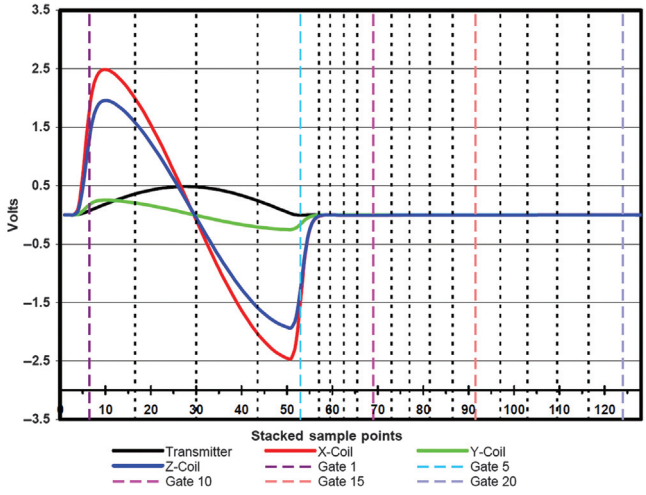

Figure 4. The primary field for the x-, y-, and z-components (the response measured at high altitude) and the transmitter current waveform. The dotted vertical lines are the centers of the window or gate positions with every fifth window being dashed, colored, and labeled in the legend. The on-time windows are 1–5, and the off-time windows are 6–20. In this paper, we only use window 1. Figure from Fugro (2005).

Figure 8 and also gridded using the minimum curvature. The terrain model shows highs (red) running north–northeast, likely glacial features such as drumlins. The areas of low terrain (blue) appear in many cases to have larger z- and x-component responses. These could be due to swamps or more conductive lacustrine sediments. Some of these trend in a different direction from the topography, for example, features trending north–south in the northwest of the survey area.

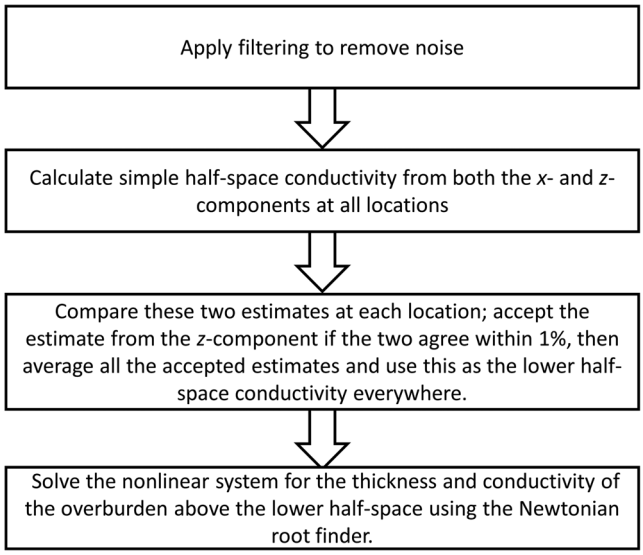

Figure 5. Flowchart summarizing processing and inversion steps.

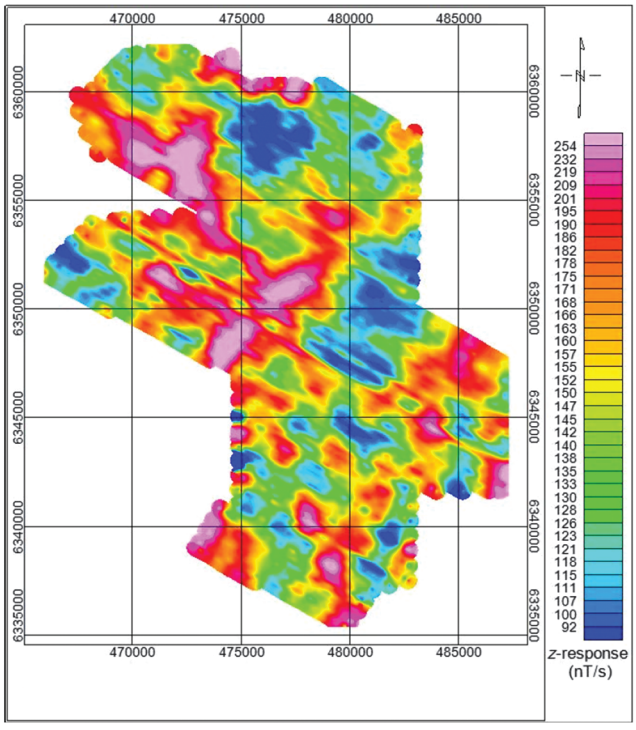

Figure 6. The z-response from the first measurement window. This and all other maps have color bars adjusted to an equal-area presentation. The observation or flight lines are parallel to the edges of the survey area running 120–300° and spaced 300 m apart.

The parameters derived from the inversion, thick-sheet conductivity and thickness, are shown in Figures 9 and 10, respectively. When these data were first gridded, unrealistic negative values of the conductivity and thickness were created in the grid. These are artifacts of the minimum curvature algorithm trying to create a smooth surface in the vicinity of a large parameter adjacent to a small parameter and as a consequence creating a negative undershoot. These artifacts were avoided in Figures 9 and 10 by using an inverse distance gridding algorithm. Note that the conductivity values shown in Figure 9 are extremely small, indicating that the on-time methods are sensitive to extremely resistive ground. Such small values are difficult to resolve with off-time data.

The conductivity and thickness maps in Figures 9 and 10 show sharper features and more detail than the z- and x-component maps in Figures 6 and 7. Some of these features might be noise or related to topographic changes. The leveling features running parallel to the lines and evident in Figures 6 and 7 have been significantly reduced, perhaps because these are related to variations in the flying height, which is taken into account by the inversion.

Comparison to casing depth of drillholes

A drillhole database was obtained from the GSS. These holes were drilled to explore for uranium deposits at hundreds of meters in depth near the unconformity below the Proterozoic Athabasca Group. There is no detailed information about the thickness or the conductivity profile of the Quaternary glacial overburden, so the drillhole database provides the only consistent information about the overburden over the survey area. The locations of the drillholes are shown in Figures 8 and 9 with small squares. We have used the casing depth as a proxy for the thickness of the overburden because it is usually unconsolidated and unstable where the casing is

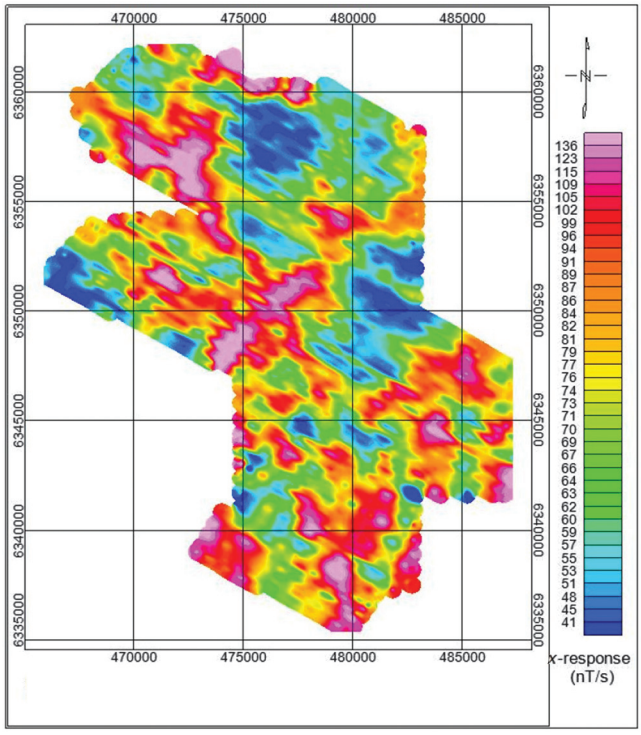

Figure 7. The x-response from the first measurement window.

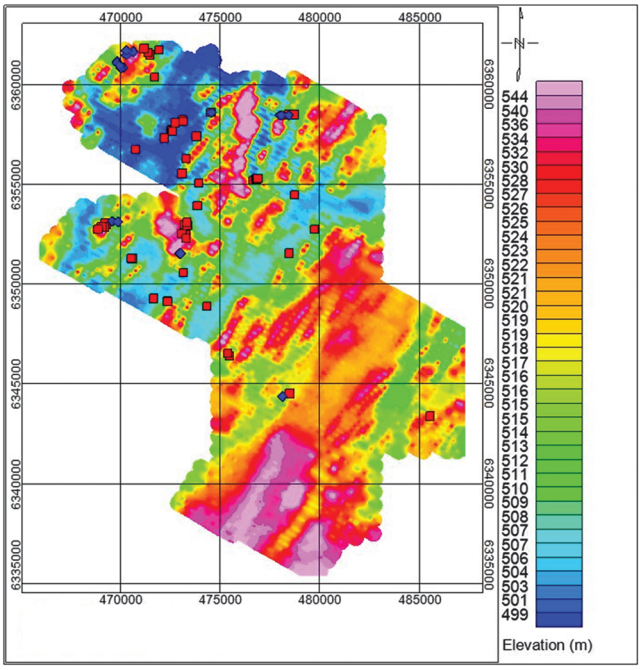

Figure 8. The DTM showing the topography of the area. The symbols are drillhole locations, divided into two populations, discussed later in the text. Population 1 is shown with blue-filled squares, and population 2 is shown with red-filled squares.

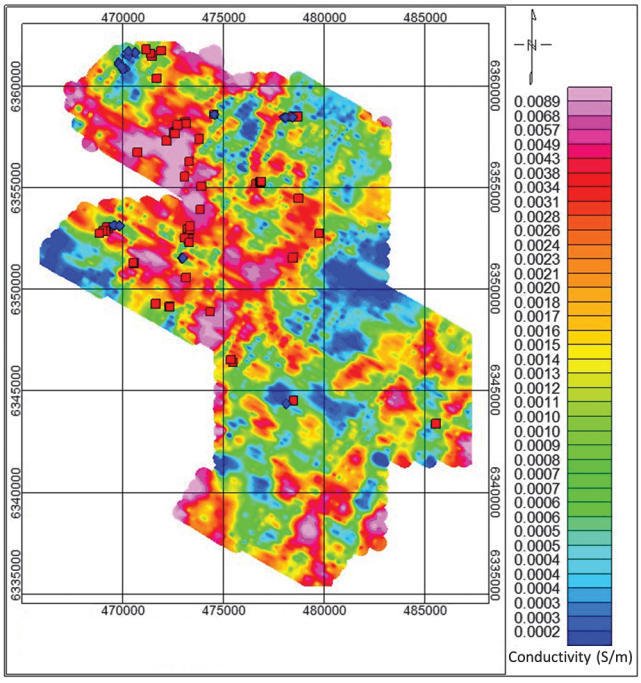

Figure 9. The thick-sheet conductivity representing the conductivity of an overburden as determined by inversion with an estimated 0.000296 S/m lower half-space conductivity. The symbols are drillhole locations, divided into two populations, discussed later in the text. Population 1 is shown with blue-filled squares, and population 2 is shown with red-filled squares.

required and hence likely to be glacial overburden. However, the casing depth is an imperfect estimate of the overburden thickness for the following reasons: (1) Borehole locations are sparse and nonrandom, generally being concentrated in more prospective areas, so they provide a poor statistical sample; (2) a casing is used where the rock is less competent, so it can be used in the shallowest part of the bedrock, which can be weathered and fractured; (3) some drillers may err on the side of safety and make the casing deeper than necessary; (4) drillholes may be far from the flight lines and may be a poor estimate of the overburden thickness at the flight line location; and (5) the location of the borehole might be incorrect, being entered using an inconsistent datum (NAD 27 instead of NAD 83).

In addition to the casing depth being a poor estimate of overburden depth, there are also assumptions made in deriving the estimate of overburden depth from the AEM data. Some of these assumptions might not always be correct, for example, (1) the lower half-space conductivity might not be uniform across the survey area, (2) the overburden to lower half-space transition might be gradual, not sudden as a two-layer model assumes, (3) the top of the conductive overburden might not begin at the terrain surface as estimated from the GPS and radar altimeter, and (4) the GEOTEM waveform at the switch on (window 1) might not be well represented by a Dirac delta function. Despite all these inadequacies a comparison was made between the inverted sheet thickness and the casing depth and shown in Figure 11. It can be seen that there are two population clusters. The first population is sparse, and the sheet thickness is about three times greater than the casing depth. The second population has more samples, and the line of best fit gives an overburden or sheet thickness that is approximately half of that which has been estimated using the casing depth.

Comparison to topography

The casing depth is a useful proxy for the thickness of the overburden; however, the distribution of the drilling is sparse. It is also

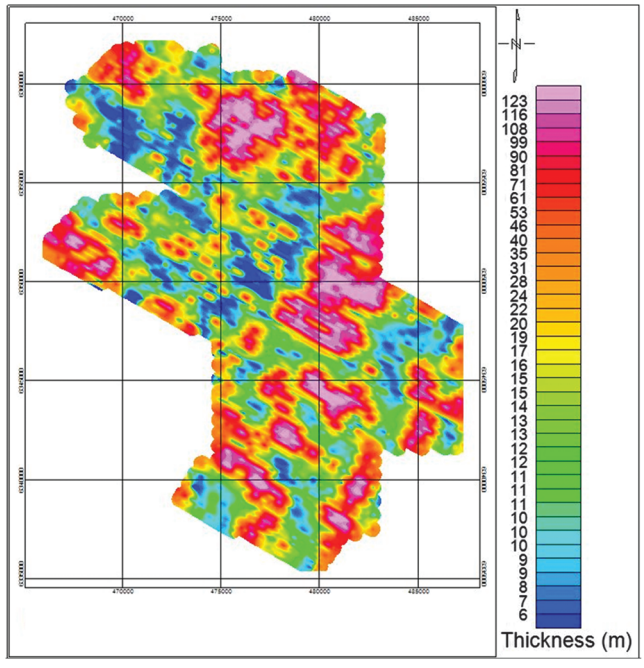

Figure 10. The thick-sheet thickness representing the thickness of conductive overburden above a 0.000296 S/m lower half-space.

DOI:10.1190/geo2021-0307.1

presumed that the exploration drilling practice will minimize the meters of overburden drilled, for example, drilling beside a drumlin rather than on top and through it, meaning that the sampling will be biased. Note that the drill locations in Figure 8 are away from the local peaks and in the local valleys, and there are no drill collars on the topographic highs. This means that the database is biased toward examples of low topography and thinner overburden (if the overburden thickness is assumed to be thicker below the topographic highs). However, the EM will be sensitive to the nearby hills and result in a greater estimate of thickness. This might explain why some thickness estimates are too deep. Furthermore, the casing depth will, in many cases, be greater than the overburden depth because the decision may be made to make the casing deeper, so as to be sure the hole will not collapse in less consolidated material.

In Figure 9, it can be seen that most of population 1 (the blue symbols) occur in areas that are resistive. Because they are less conductive, the conductivity is close to that of the bedrock and the contrast between the overburden and bedrock is poor. In these areas, the assumption of a conductor over a resistor will be poor; essentially, the geoelectric structure is a half-space and the depth to the interface will be poorly constrained, so the algorithm seems to push it too deep. The second population is mostly in the areas where the conductivity is higher.

DISCUSSION

Figures 6, 7, and 9 show that the conductivity of the thick sheet correlates somewhat with the z- and x-responses. Hence, the magnitude of these responses is what determines the conductivity. The thickness of the sheet is a more complex relationship between the relative magnitude of the x- and z-responses. For example, when an x-response is relatively strong in comparison to the z-response, a thick sheet is interpreted on top of the lower half-space.

The DTM in Figure 8 may be compared to the inverted sheet thickness in Figure 10. By comparison, the inverted sheet thickness is smeared, with longer wavelength features that are broad. Overall, the thickness generally shows that the thinner areas are associated with the more conductive features that have the stronger responses in the z- and x-component responses. Conversely, the thicker areas are the areas with smaller responses and are more resistive. In these latter areas, a resistive half-space model might be more appropriate,

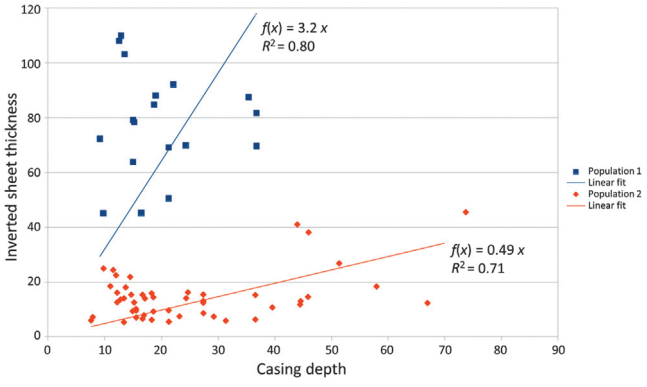

Figure 11. Comparison between inverted sheet thickness (the vertical axis) and casing depth, a proxy for overburden thickness (the horizontal axis). Two populations have been fitted to a line of best fit with a zero intercept. Red population 2 and blue population 1.

so the thick layer model might not be appropriate and the depth might be poorly resolved (see Appendix A of Bagley and Smith, 2018).

The casing thickness from drilling was used as a proxy for overburden thickness, which was compared with the inverted sheet thickness in Figure 11. Neither population has a strong correlation to the sheet thickness, although the second population has a much lower R^2 than the first. Figure 9 shows the location of population 1 with blue symbols and population 2 is shown with red symbols. These two populations are interpreted to correspond to the resistive and conductive areas, respectively. These conductive units might be clays or glaciolacustrine units within the overburden. The conductive units could be anywhere between the surface and the base of the overburden, which is consistent with the thickness being less than the overburden casing depth (the line with a slope of 1 in Figure 11).

For the field example presented in this paper, the ground is extremely resistive over a large portion of the area, so resistive-limit methods were critical because only the on-time data had a reasonable signal over a large portion of the area. It was also important to have a fair estimate of the conductivity of the lower half-space because this is comparable to the overburden in some locations. Hence, our field example demonstrated the application of the model comprising a thick layer over a lower half-space where we had to estimate the conductivity of the lower half-space. This is our most complicated model. However, in other circumstances, it may be appropriate to make assumptions that mean that one or more of the other simple models that we have introduced in this paper can be used. For example, Smith and Lee (2021) use the depth and conductance of the thin-sheet model as an initial guess for an inversion involving a more complicated model that varies smoothly with depth.

CONCLUSION

The 2C resistive-limit data allow two parameters of the ground to be resolved simply. Models that are completely described by two parameters are

1) the conductance and depth of a thin layer
2) the depth to and conductivity of a half-space
3) the conductance of a thin layer at the surface and the conductivity of an underlying lower half-space
4) the conductivity and thickness of a thick layer at a surface above an infinitely resistive basement.

A two-layer earth is completely described by three parameters (the upper and lower conductivity and the depth to the interface). If one of the parameters is assumed, then the following models can be resolved:

5) the conductivity above and below an interface at an assumed depth
6) the depth to and conductivity of a layer below an upper layer of assumed conductivity
7) the thickness and conductivity of a layer above a lower half-space of assumed conductivity.

The thick sheet, case 4, is a special case of case 7 in which the lower half-space conductivity is assumed to be zero. Cases 4, 6, and 7 require that the root of an equation be solved to determine the depth to an interface. In cases 1 and 2, the estimated depth to the thin sheet or half-space can be compared with the aircraft altimeter, and if the depth is greater than the altimeter and the conductance or

conductivity is positive, then this provides some certainty that the assumed model is reasonable. At locations where the half-space solution seems reasonable, the estimated conductivity can then be used to estimate and extrapolate a third parameter, the assumed value for the lower half-space below the thick-sheet model. The thick-sheet model can then be solved with an equation solver for sheet thickness and conductivity. In this way, a third model parameter can be teased from the 2C data.

These simple models assume that the data are in the resistive limit, which should be approximately true if the apparent conductance is less than 20 S or the apparent conductivity is less than 0.02 S/m. If the apparent conductance or conductivity is significantly less than these values, then the approximation will be much better.

When applied to real-world data from the Athabasca Basin, case 7 seemed most appropriate and the results that we obtained were encouraging. This example also illustrated some of the complexities of working with real data. Where the response is small and noisy, the estimate of the thickness of the overburden was too deep and unreliable. In general, these areas are resistive, with conductivities comparable to the lower half-space, so the thickness is poorly constrained by the data. Where the response was large, the estimate was more reliable but generally shallower than expected, most likely because the conductive material was above the overburden as estimated from the casing depth. Where the signal is adequate, the estimated overburden thickness sometimes reflects topography and at other times shows distinct features, suggesting that these features are consistent with and determined by the measured AEM response.

If a survey area is a layer over a half-space, then one of our models or a combination of the models could be used to extract useful information from EM data.

ACKNOWLEDGMENTS

We are grateful to NSERC for funding this research and to R. Hearst (Southern Geoscience Consultants, formerly with AREVA [now ORANO] Canada Resources Inc) and L. Petrie (Denison Mines) for encouraging this avenue of research. The Fugro reports can be found on the Saskatchewan Mineral Assessment Database by searching for digital submissions from 2005 lodged by Roughrider Uranium under assessment file number 74H06-0127. They can also be obtained from the corresponding author R. Smith.

DATA AND MATERIALS AVAILABILITY

Data associated with this research are available and can be accessed via the following URL: http://mineral-assessment.saskatchewan.ca/Pages/BasePages/Main.aspx.

REFERENCES

Annan, A. P., R. S. Smith, J. Lemieux, M. D. O'Connell, and R. N. Pedersen, 1996, Resistive-limit time-domain AEM conductivity: Geophysics, **61**, 93–99, doi: 10.1190/1.1443960.

Bagley, T. E., and R. S. Smith, 2018, Estimating overburden thickness in resistive areas from two-component airborne EM data: 88th Annual International Meeting, SEG, Expanded Abstracts, 1893–1897, doi: 10.1190/segam2018-2998300.1.

Braine, M. F., and J. C. Macnae, 1999, Removing the regolith: EM defined structure fails to correct gravity at Elura: Exploration Geophysics, **30**, 115–122, doi: 10.1071/EG999115.

Darijani, M., 2019, Investigating modelling and inversion techniques for overburden stripping for uranium exploration in the Athabasca Basin, Canada: Ph.D. thesis, Memorial University of Newfoundland.

Edwards, R. N., and S. J. Cheesman, 1987, Two-dimensional modeling of a towed transient magnetic dipole-dipole sea floor EM system: Journal of Geophysics, **61**, 110–121.

Fugro, 2005, Logistics and processing report, airborne magnetic and GEOTEM survey, Russell South & Russell West Saskatchewan, Job no. 05407: Technical report, Fugro Airborne Surveys Corp.

Grant, F. S., and G. F. West, 1965, Interpretation theory in applied geophysics: McGraw-Hill.

Jefferson, C. W., D. J. Thomas, S. S. Gandhi, P. Ramaekers, G. Delaney, D. Brisbin, C. Cutts, P. Portella, and R. A. Olson, 2007, Unconformity-associated uranium deposits of the Athabasca Basin, Saskatchewan and Alberta, *in* C. W. Jefferson and G. Delaney, eds., EXTECH IV: Geology and uranium exploration technology of the Proterozoic Athabasca Basin, Saskatchewan and Alberta: Geological Survey of Canada Bulletin 588, 23–67.

Parker, R. L., 1977, The fréchet derivative for the one-dimensional electromagnetic induction problem: Geophysical Journal International, **49**, 543–547, doi: 10.1111/j.1365-246X.1977.tb03723.x.

Robertshaw, P., 2006, Report on a 2005 GEOTEM survey Russell South property, northern Saskatchewan on behalf of Roughrider Uranium Corp.: Technical report, Robertshaw Geophysics Ltd.

Smith, R., 2001, On removing the primary field from fixed-wing time-domain airborne electromagnetic data: Some consequences for quantitative modelling, estimating bird position and detecting perfect conductors: Geophysical Prospecting, **49**, 405–416, doi: 10.1046/j.1365-2478.2001.00266.x.

Smith, R. S., 2000, The realizable resistive limit: A new concept for mapping geological features spanning a broad range of conductivities: Geophysics, **65**, 1124–1127, doi: 10.1190/1.1444805.

Smith, R. S., R. N. Edwards, and G. Buselli, 1994, An automatic technique for presentation of coincident-loop, impulse response, transient, electromagnetic data: Geophysics, **59**, 1542–1550, doi: 10.1190/1.1443543.

Smith, R. S., and T. J. Lee, 2021, Multiple-order moments of the transient electromagnetic response of a one-dimensional earth with finite conductance — The Gaussian variation applied to a field example: Exploration Geophysics, **52**, 1–13, doi: 10.1080/08123985.2021.1925105.

Smith, R. S., T. J. Lee, A. P. Annan, and M. D. O'Connell, 2005, Approximate apparent conductance (or conductivity) from the realizable moments of the impulse response: Geophysics, **70**, no. 1, G29–G32, doi: 10.1190/1.1852776.

Wait, J. R., 1982, Geoelectromagnetism: Academic Press.

Ward, S. H., 1967, Electromagnetic theory for geophysical applications, *in* W. E. Heinrichs, R. C. Holmer, R. E. MacDougall, G. R. Rogers, J. S. Sumner, and S. H. Ward, eds., Mining geophysics, Volume 2, theory: SEG 2, 13–196.

Biographies and photographs of the authors are not available.